

# Supplemental Materials: Position-free Multiple-bounce Computations for Smith Microfacet BSDFs

BEIBEI WANG, Nankai University, China

WENHUA JIN, JIAHUI FAN, Nanjing University of Science and Technology, China

JIAN YANG, Nankai University, China

NICOLAS HOLZSCHUCH, University Grenoble Alpes, Inria, CNRS, Grenoble INP, LJK, France

LING-QI YAN, University of California, Santa Barbara, USA

## 1 FULL SPHERICAL SHADOWING-MASKING FUNCTION

In this section, we provide proofs and analysis for our height-uncorrelated and height-correlated shadowing-masking functions.

### 1.1 Height-uncorrelated shadowing-masking function

As illustrated in Fig. 1, in the upper hemisphere, the projected area of microfacets towards direction  $\omega$  can be written in the integral form as

$$\text{projected area} = \omega \cdot \omega_g = \int_{\Omega^+} G_1(\omega, \omega_m) \langle \omega, \omega_m \rangle D(\omega_m) d\omega_m, \quad (1)$$

where  $G_1$  determines whether a microfacet will contribute to the projected area. And two possible non-contributing cases are (1) locally, a microfacet has a backward orientation w.r.t. the given direction  $\omega$ , and (2) distantly, a microfacet will be occluded by other microfacets regardless of its own orientation  $\omega_m$ .

Using the local / distant separated form of  $G_1$  and taking advantage of the distant term  $G_1^{\text{dist}}$ 's independence of any microfacet's normal, Eqn. 1 can be solved [Heitz et al. 2016] in the following form:

$$G_1^{\text{dist}}(\omega) = \frac{1}{1 + \Lambda(\omega)}, \quad (2)$$

where  $\Lambda$  is computed from the normal distribution function by integrating, as described by Smith [1967].

However, when the direction of interest  $\omega$  is from below the surface, Eqn. 1 does not hold anymore, since  $\omega \cdot \omega_g$  will be negative. Our first goal is to extend Eqn. 1 to handle this case. This is done by replacing the projected area with  $|\omega \cdot \omega_g|$ , so the projected area is always positive and is physically correct no matter which direction of interest  $\omega$  is provided. This leads to our spherical distant shadowing / masking term:

$$G_1^{\text{dist}}(\omega) = \left| \frac{1}{1 + \Lambda(\omega)} \right| = \begin{cases} 1/(1 + \Lambda(\omega)), & \text{if } \omega \cdot \omega_g > 0, \\ -1/(1 + \Lambda(\omega)), & \text{if } \omega \cdot \omega_g \leq 0, \end{cases} \quad (3)$$

In Fig. 2, we validate the correctness of Eqn. 3, by comparing with the numerical solution of the integral form of  $G_1^{\text{dist}}(\omega)$  derived from

Authors' addresses: Beibei Wang, Nankai University, China, beibei.wang@nankai.edu.cn; Wenhua Jin, Jiahui Fan, Nanjing University of Science and Technology, China, jwh.fjh@njjust.edu.cn; Jian Yang, Nankai University, China, csjyang@nankai.edu.cn; Nicolas Holzschuch, University Grenoble Alpes, Inria, CNRS, Grenoble INP, LJK, France, nicolas.holzschuch@inria.fr; Ling-Qi Yan, University of California, Santa Barbara, USA, lingqi@cs.ucsb.edu.

our extended spherical form of Eqn. 1:

$$G_1^{\text{dist}}(\omega) = \frac{|\omega \cdot \omega_g|}{\int_{\Omega^\pm} G_1^{\text{local}}(\omega, \omega_m) \langle \omega, \omega_m \rangle D(\omega_m) d\omega_m}. \quad (4)$$

As expected, the two solutions match very well. The curves for other configurations (other NDFs, like Beckmann or other roughness) also match well.

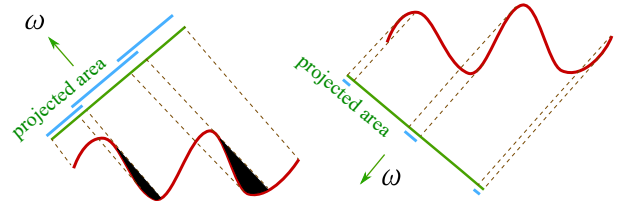


Fig. 1. For both  $\omega$  from above the macrosurface (left) or from below the macrosurface (right), the blue area represents the projected area of microfacets which are not back-facing, without considering shadowing, and the green area represents the projected area considering shadowing, thus  $G_1^{\text{dist}}$  is the ratio between the areas of blue and green.

One important and interesting observation, is that when  $\omega$  is from below the macrosurface, the value of  $G_1^{\text{dist}}$  could be greater than 1. This observation can be strictly validated by re-looking at Fig. 1. As illustrated, the entire shadowing / masking term  $G_1$  gives the projected area, marked as green, while if we ignore the shadowing between microfacets, i.e., project a microfacet as long as it's not back-facing, we will end up with the blue area, predicted only by  $G_1^{\text{local}}$ . By its mathematical definition,  $G_1^{\text{dist}}$  is the ratio between the areas of blue and green.

When projecting upwards, since there will never be holes on a surface, the blue area is always guaranteed to be not smaller than the green area. Therefore, the distant shadowing / masking term only performs pruning in this case. However, when projected downwards, very few microfacets are front-facing w.r.t.  $\omega$ , and therefore cannot pass the local test. This results in much smaller blue area. In this case, the  $G_1^{\text{dist}}$  term should be greater than 1.

### 1.2 Height-correlated shadowing-masking function

As shown in Ross et al. [2005], the height-correlated shadowing-masking function for reflection is:

$$G_2^{\text{dist}}(\omega_i, \omega_o) = \frac{1}{1 + \Lambda(\omega_i) + \Lambda(\omega_o)}, \quad (5)$$

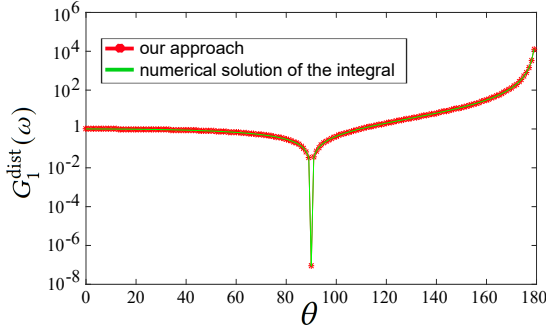


Fig. 2. We validate our spherical distant shadowing / masking term  $G_1^{\text{dist}}(\omega)$  computed with our Eqn. 3 against the numerical solution of Eqn. 6.  $G_1^{\text{dist}}(\omega)$  is visualized logarithmically as a function of the angle  $\theta$  between  $\omega$  and  $\omega_g$ . NDF: GGX model with  $\alpha = 1.0$ .

where both  $\omega_i$  and  $\omega_o$  are above the macrosurface.

To extend Eqn. 5 to the full-spherical domain, we first derive the integral form of  $G_2^{\text{dist}}(\omega_i, \omega_o)$  by :

$$\begin{aligned} & 1 + \Lambda(\omega_i) + \Lambda(\omega_o) \\ &= \frac{\int_{\Omega^+} \langle \omega_i, \omega_m \rangle D(\omega_m) d\omega_m}{\omega_i \cdot \omega_g} + \frac{\int_{\Omega^+} \langle -\omega_o, \omega_m \rangle D(\omega_m) d\omega_m}{\omega_o \cdot \omega_g} \\ &= \frac{\int_{\Omega^+} D(\omega_m) [\langle \omega_i, \omega_m \rangle (\omega_o \cdot \omega_g) + \langle -\omega_o, \omega_m \rangle (\omega_i \cdot \omega_g)] d\omega_m}{(\omega_i \cdot \omega_g)(\omega_o \cdot \omega_g)}, \end{aligned} \quad (6)$$

$$\begin{aligned} & \frac{1}{1 + \Lambda(\omega_i) + \Lambda(\omega_o)} \\ &= \frac{(\omega_i \cdot \omega_g)(\omega_o \cdot \omega_g)}{\int_{\Omega^+} D(\omega_m) [\langle \omega_i, \omega_m \rangle (\omega_o \cdot \omega_g) + \langle -\omega_o, \omega_m \rangle (\omega_i \cdot \omega_g)] d\omega_m} \end{aligned} \quad (7)$$

where  $\omega_i$  and  $\omega_o$  are still above the macrosurface.

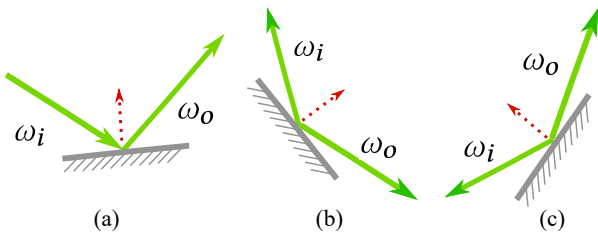


Fig. 3. There are only three cases in the reflection case: (a) both the incoming and outgoing directions point to the the upper hemisphere of the macrosurface; (b) only the incoming direction points to the the upper hemisphere of the macrosurface; (c) only the outgoing direction points to the the upper hemisphere of the macrosurface.

One importance observation is that only one of the directions could be below the macrosurface in the reflection case. As shown in Fig. 3, since the microfacet is a single-sided facet, and the normal of the front-side of the microfacet will always point to the upper

hemisphere of the macrosurface. When both the incoming and the outgoing directions are below the macrosurface, the half vector or the microsurface normal is also below the macrosurface. This will conflict with the previous claim.

Since only one of the directions could be below the macrosurface, we assume it's the incoming direction for simplicity. Starting from Eqn. 7, we have:

$$\begin{aligned} & \int_{\Omega^+} D(\omega_m) [\langle \omega_i, \omega_m \rangle (\omega_o \cdot \omega_g) + \langle -\omega_o, \omega_m \rangle (\omega_i \cdot \omega_g)] d\omega_m \\ &= (1 + \Lambda(\omega_i) + \Lambda(\omega_o)) (\omega_i \cdot \omega_g) (\omega_o \cdot \omega_g). \end{aligned} \quad (8)$$

If the incoming direction is below the macrosurface, and we denote it as  $-\omega_i$ , then we have:

$$\begin{aligned} & \int_{\Omega^+} D(\omega_m) [\langle -\omega_i, \omega_m \rangle (\omega_o \cdot \omega_g) + \langle -\omega_o, \omega_m \rangle (\omega_i \cdot \omega_g)] d\omega_m \\ &= (\Lambda(\omega_i) (\omega_i \cdot \omega_g) (\omega_o \cdot \omega_g) + \Lambda(\omega_o) (\omega_i \cdot \omega_g) (\omega_o \cdot \omega_g)), \\ &= (\Lambda(\omega_i) + \Lambda(\omega_o)) (\omega_i \cdot \omega_g) (\omega_o \cdot \omega_g), \end{aligned} \quad (9)$$

thus, we get:

$$G_2^{\text{dist}}(-\omega_i, \omega_o) = \frac{1}{\Lambda(\omega_i) + \Lambda(\omega_o)}, \text{ if } \omega_i \cdot \omega_g > 0 \quad (10)$$

If we use  $\omega_i$  to denote the direction below the macrosurface, we have the equivalence formulation:

$$G_2^{\text{dist}}(\omega_i, \omega_o) = \frac{1}{\Lambda(-\omega_i) + \Lambda(\omega_o)}, \text{ if } \omega_i \cdot \omega_g < 0. \quad (11)$$

Now we have the complete definition of the height-correlated shadowing-masking function:

$$G_2^{\text{dist}}(\omega_i, \omega_o) = \begin{cases} \frac{1}{-\Lambda(-\omega_i) + \Lambda(\omega_o)}, & \text{if } \omega_i \cdot \omega_g > 0, \\ \frac{1}{\Lambda(-\omega_i) + \Lambda(\omega_o)}, & \text{if } \omega_i \cdot \omega_g \leq 0. \end{cases} \quad (12)$$

The height-correlated shadowing-masking function for the last bounce is the same as the height-correlated shadowing-masking function:

$$G_2^{i=k}(\omega_i, \omega_o) = G_2^{\text{dist}}(\omega_i, \omega_o). \quad (13)$$

### 1.3 Height-correlated shadowing-masking function for the middle bounce

For the middle bounce, the shadowing-masking function has different meaning from the last bounce. For bounce  $i$  ( $i < k$ ), shadowing-masking function  $G_2^{i < k}(\omega_i, \omega_o)$  means the probability that the light ray with incident direction  $\omega_i$  arrives at the surface and the outgoing ray with direction  $\omega_o$  is blocked.

If  $\omega_o$  is below the macrosurface, the ray will always intersect with the microgeometry, resulting in

$$G_2^{i < k}(\omega_i, \omega_o) = \frac{1}{1 + \Lambda(\omega_i)}, \text{ if } \omega_o \cdot \omega_g < 0. \quad (14)$$

If  $\omega_o$  is above the macrosurface, we derive a novel formulation. Starting from the original definition of the height-correlated shadowing-masking function [Heitz et al. 2016]:

$$G_2^{\text{dist}}(\omega_i, \omega_o) = \int_{-\infty}^{+\infty} G_1^{\text{dist}}(\omega_i, h) G_1^{\text{dist}}(\omega_o, h) P^1(h) dh, \quad (15)$$

where  $P^1(h)$  is the height distribution function.

We propose a novel formulation for the middle bounce from Eqn. 15 :

$$\begin{aligned}
 & G_2^{i < k}(\omega_i, \omega_o) \\
 &= \int_{-\infty}^{+\infty} G_1^{\text{dist}}(\omega_i, h)(1 - G_1^{\text{dist}}(\omega_o, h))P^1(h)dh, \\
 &= \int_{-\infty}^{+\infty} G_1^{\text{dist}}(\omega_i, h)P^1(h)dh - \int_{-\infty}^{+\infty} G_1^{\text{dist}}(\omega_i, h)G_1^{\text{dist}}(\omega_o, h)P^1(h)dh, \\
 &= G_1^{\text{dist}}(\omega_i) - G_2^{\text{dist}}(\omega_i, \omega_o), \\
 &= \frac{1}{|\Lambda(\omega_i) + 1|} - \frac{1}{|\Lambda(-\omega_i)| + \Lambda(\omega_o)}. \tag{16}
 \end{aligned}$$

Thus, the complete formulation of the middle bounce is:

$$G_2^{i < k}(\omega_i, \omega_o) = \begin{cases} \frac{1}{|\Lambda(\omega_i) + 1|} - \frac{1}{|\Lambda(-\omega_i)| + \Lambda(\omega_o)}, & \text{if } \omega_o \cdot \omega_g > 0, \\ \frac{1}{|\Lambda(\omega_i) + 1|}, & \text{if } \omega_o \cdot \omega_g \leq 0. \end{cases} \tag{17}$$

## 2 RECIPROCITY OF OUR MODELS

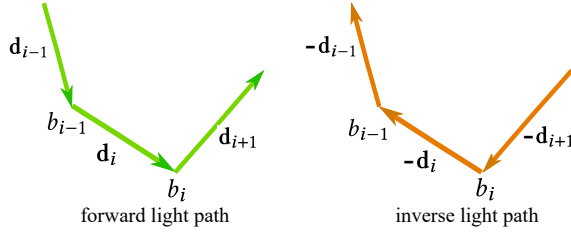


Fig. 4. A subpath ( $\mathbf{d}_{i-1}$  to  $\mathbf{d}_{i-1}$ ) from the forward light path (green) and its inverse (orange).

In this section, we analyze the reciprocity of our models (height-uncorrelated and height-correlated). We first prove that height-uncorrelated model has reciprocity, and then provide a counter example to show that our height-correlated model doesn't have reciprocity.

### 2.1 Reciprocity of our height-uncorrelated model

As shown in Section 3.4, it's obvious that the vertex terms have reciprocity. Here, we prove the reciprocity of the segment term. Since we are using a separable model for the shadowing-masking function, the product of the shadowing terms of incident direction  $\omega_i$  and exit direction  $\omega_o$  have reciprocity, given any light paths. Thus, without loss of generality, we only proof the reciprocity of the internal direction.

Given a direction  $\mathbf{d}_i$  in the forward path, as shown in Fig. 4 (left), its segment term is computed by:

$$s_i^{\text{forward}} = e_i p_i, \tag{18}$$

where  $e_i = 1$ , since the direction is below the macrosurface, and  $p_i$  is defined as:

$$p_i = G_1(-\mathbf{d}_i, \frac{-\mathbf{d}_i + \mathbf{d}_{i+1}}{\|-\mathbf{d}_i + \mathbf{d}_{i+1}\|}) = G_1^{\text{dist}}(-\mathbf{d}_i). \tag{19}$$

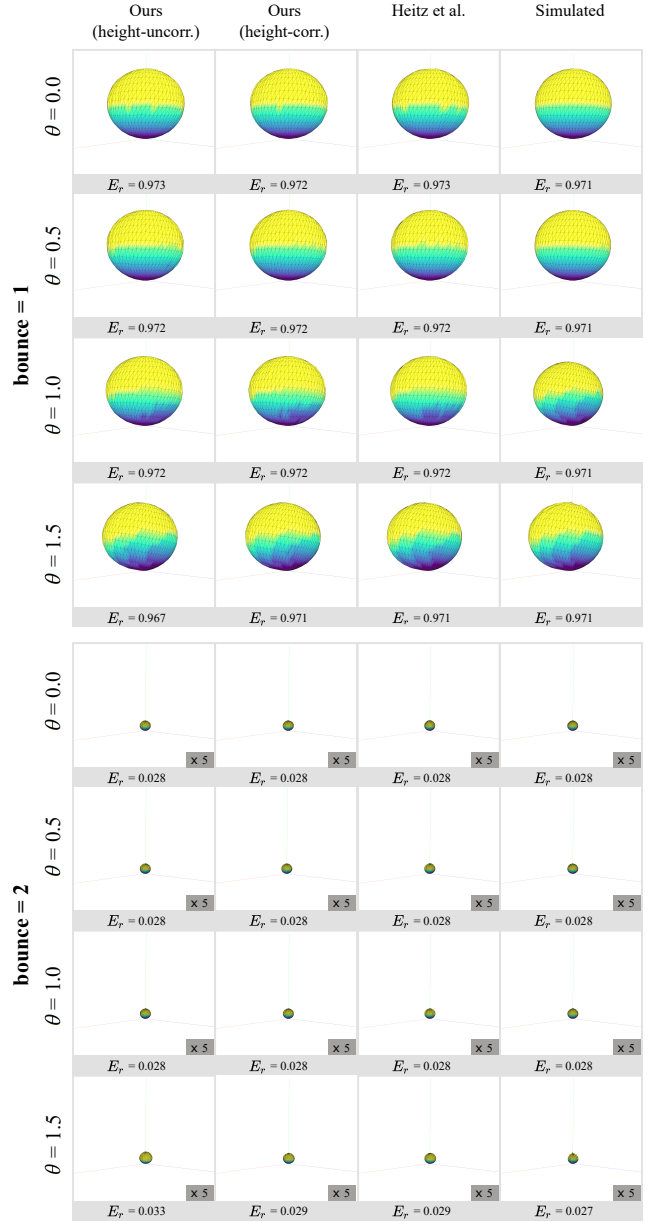


Fig. 5. Comparison between our multiple-bounce BSDF models (both height-uncorrelated and height-correlated), Heitz et al. [2016] model and simulated data, for rough diffuse material with roughness 0.25.  $\theta$  is the angle between the incident direction and the normal to the macrosurface.

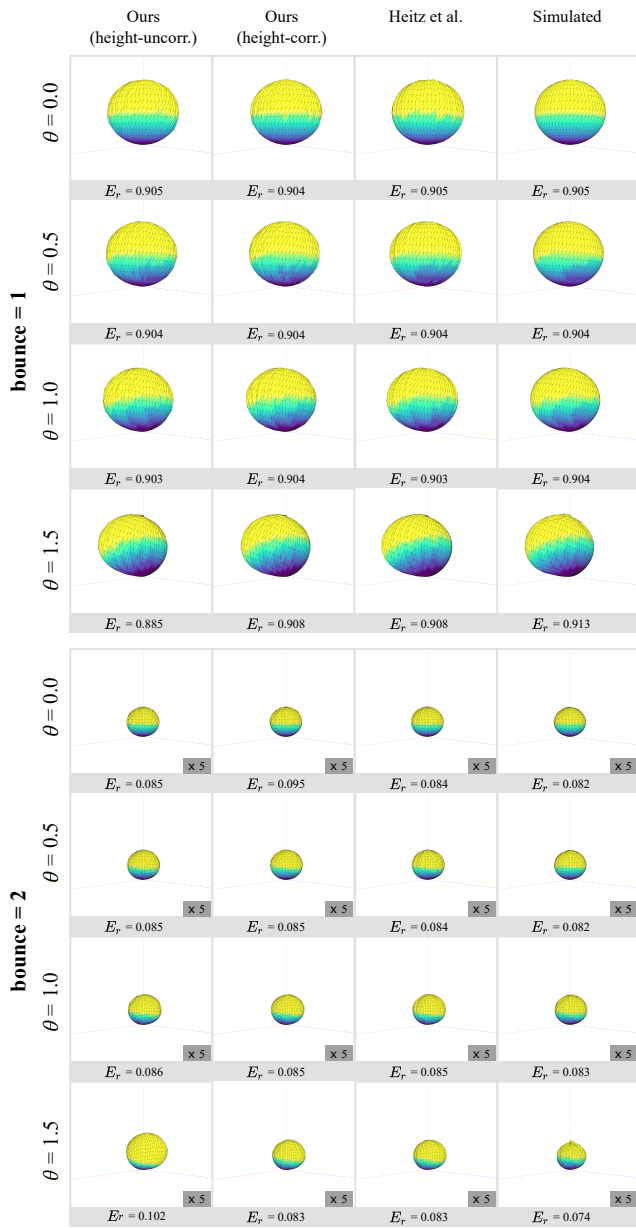


Fig. 6. Comparison between our multiple-bounce BxDF models (both height-uncorrelated and height-correlated), Heitz et al. [2016] model and simulated data, for rough diffuse material with roughness 0.5.  $\theta$  is the angle between the incident direction and the normal to the macrosurface.

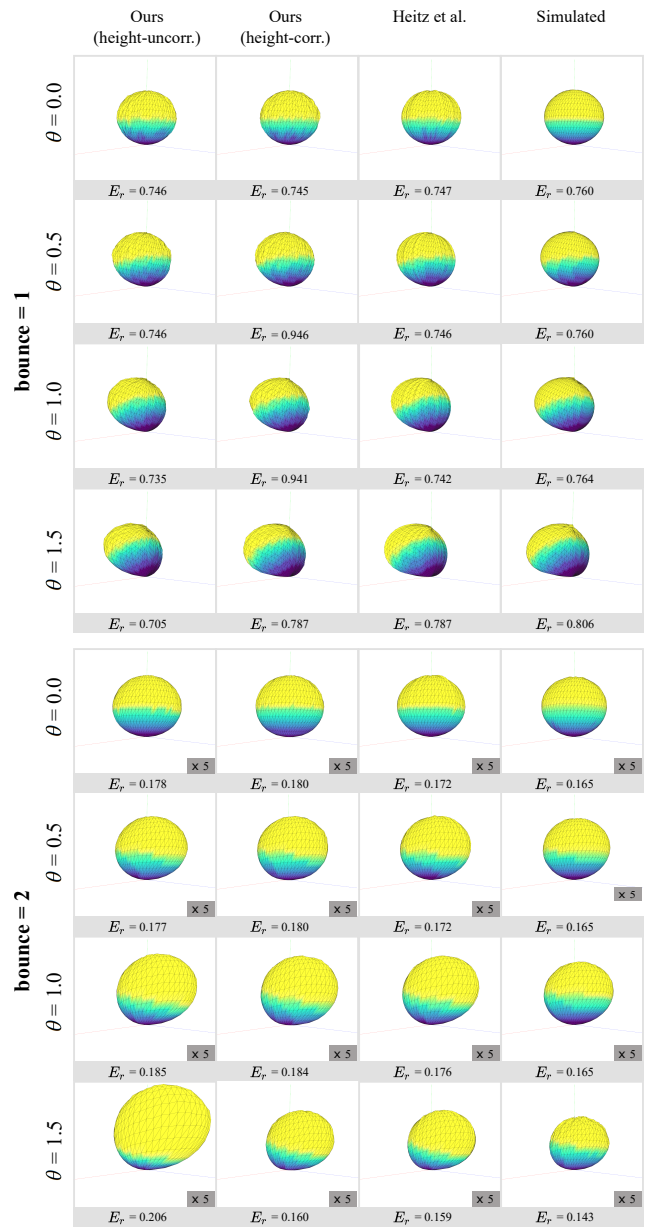


Fig. 7. Comparison between our multiple-bounce BxDF models (both height-uncorrelated and height-correlated), Heitz et al. [2016] model and simulated data, for rough diffuse material with roughness 1.0.  $\theta$  is the angle between the incident direction and the normal to the macrosurface.

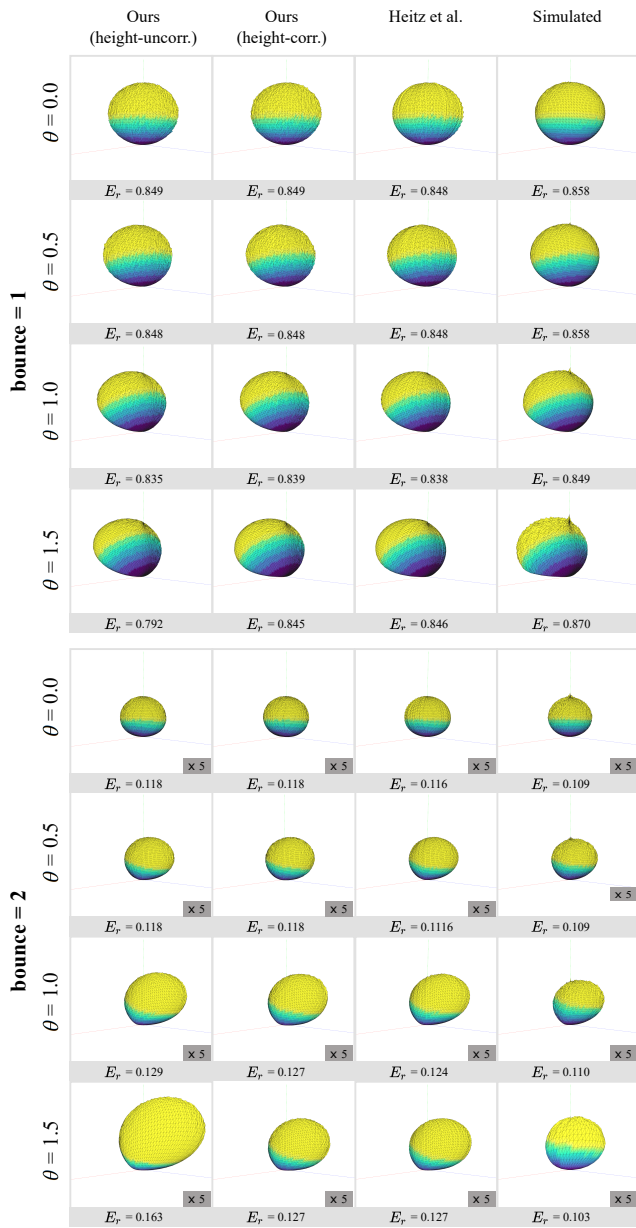


Fig. 8. Comparison between our multiple-bounce BSDF models (both height-uncorrelated and height-correlated), Heitz et al. [2016] model and simulated data, for anisotropic rough diffuse material with roughness 1.0 and 0.1.  $\theta$  is the angle between the incident direction and the normal to the macrosurface.

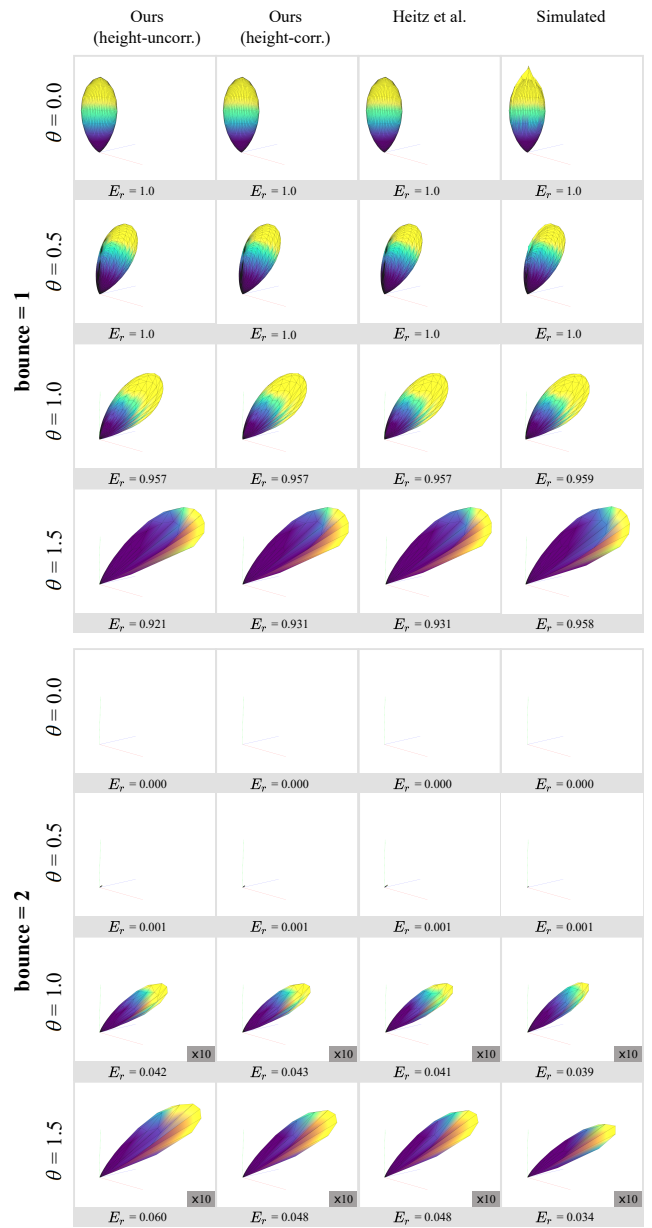


Fig. 9. Comparison between our multiple-bounce BSDF models (both height-uncorrelated and height-correlated), Heitz et al. [2016] model and simulated data, for rough conductor material with roughness 0.25.  $\theta$  is the angle between the incident direction and the normal to the macrosurface.

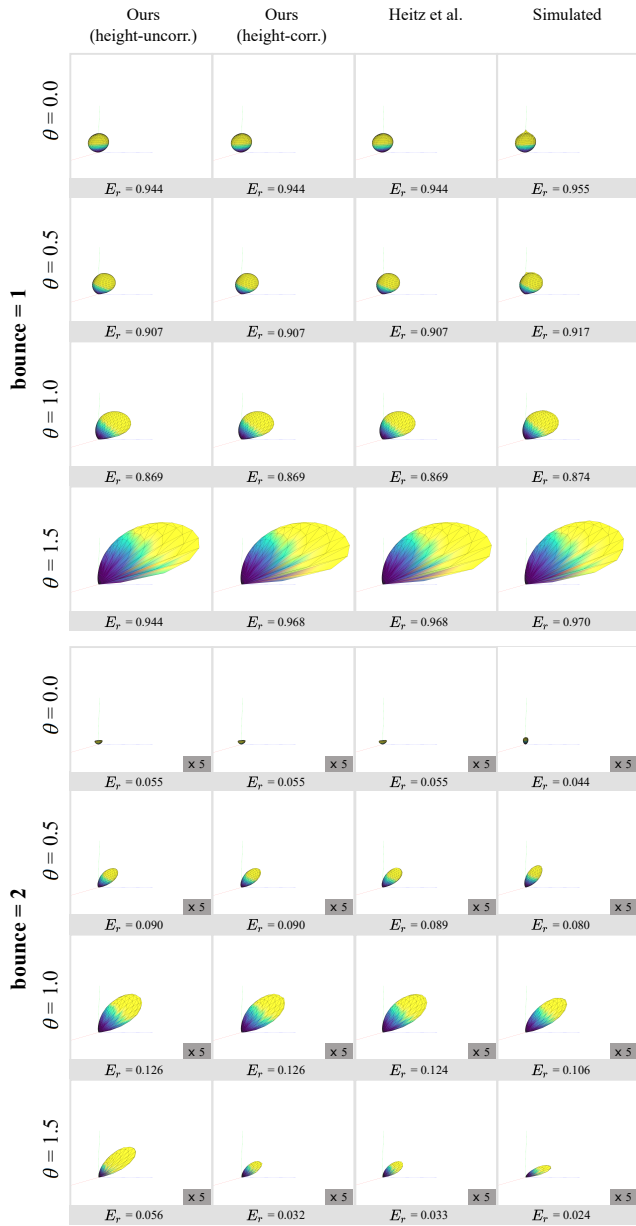


Fig. 10. Comparison between our multiple-bounce BxDF models (both height-uncorrelated and height-correlated), Heitz et al. [2016] model and simulated data, for rough conductor material with roughness 0.5.  $\theta$  is the angle between the incident direction and the normal to the macrosurface.

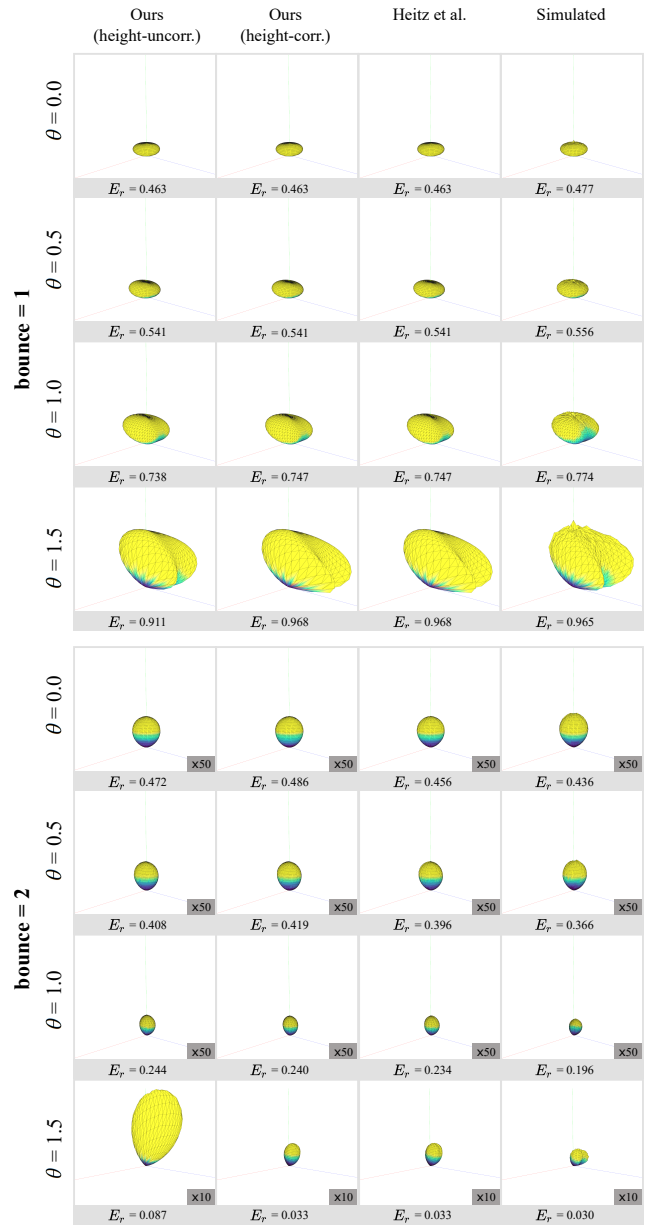


Fig. 11. Comparison between our multiple-bounce BxDF models (both height-uncorrelated and height-correlated), Heitz et al. [2016] model and simulated data, for rough conductor material with roughness 1.0.  $\theta$  is the angle between the incident direction and the normal to the macrosurface.

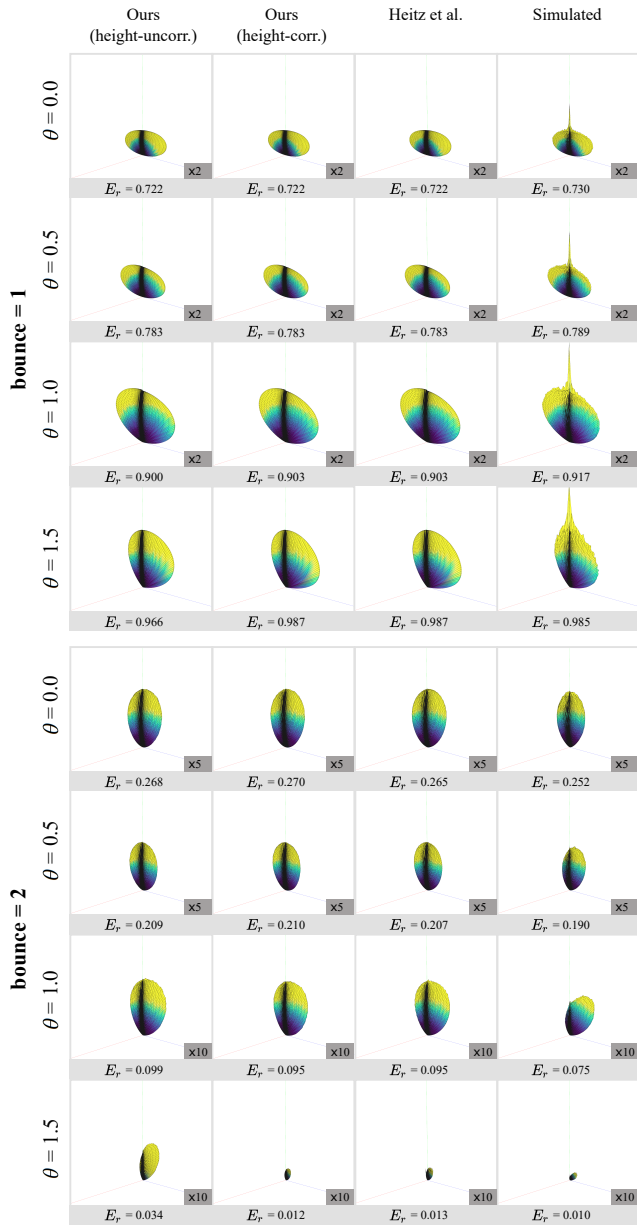


Fig. 12. Comparison between our multiple-bounce BSDF models (both height-uncorrelated and height-correlated), Heitz et al. [2016] model and simulated data, for anisotropic rough conductor material with roughness 1.0 and 0.1.  $\theta$  is the angle between the incident direction and the normal to the macrosurface.

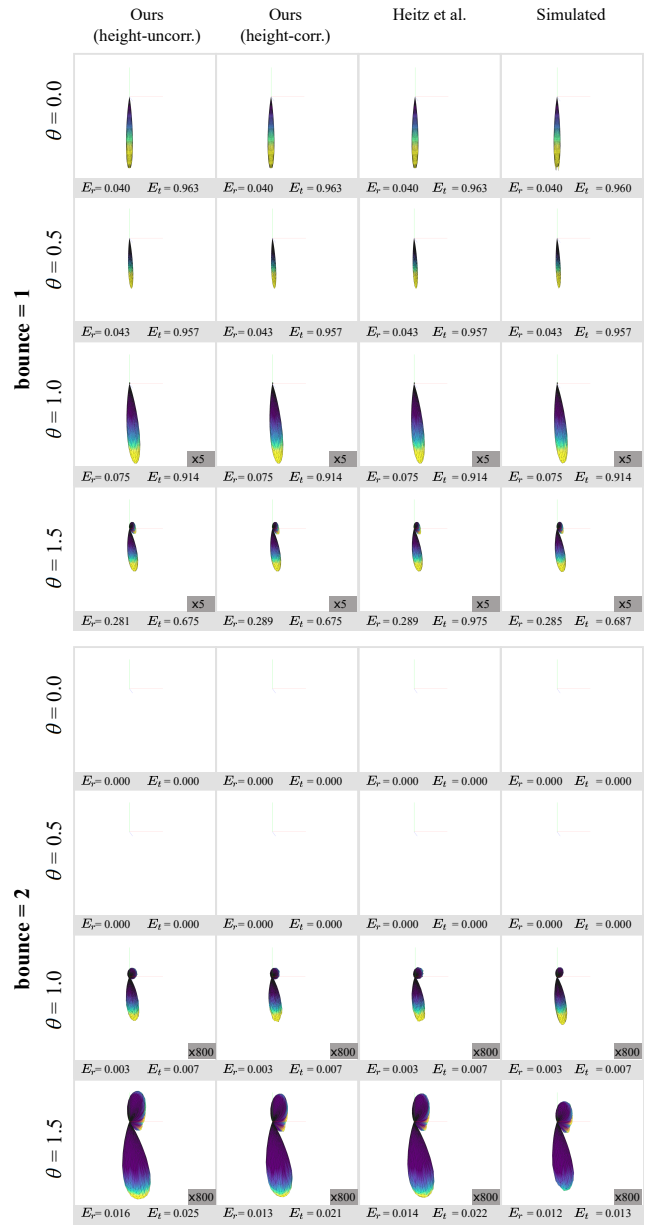


Fig. 13. Comparison between our multiple-bounce BSDF models (both height-uncorrelated and height-correlated), Heitz et al. [2016] model and simulated data, for rough dielectric material with roughness 0.25.  $\theta$  is the angle between the incident direction and the normal to the macrosurface.

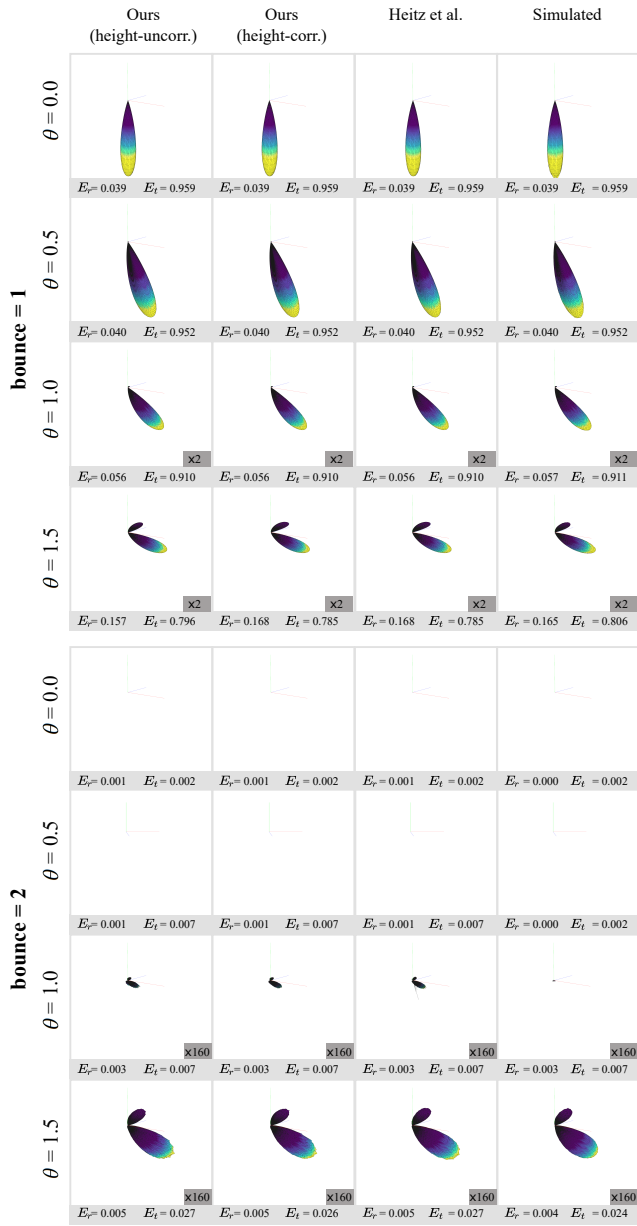


Fig. 14. Comparison between our multiple-bounce BxDF models (both height-uncorrelated and height-correlated), Heitz et al. [2016] model and simulated data, for rough dielectric material with roughness 0.5.  $\theta$  is the angle between the incident direction and the normal to the macrosurface.

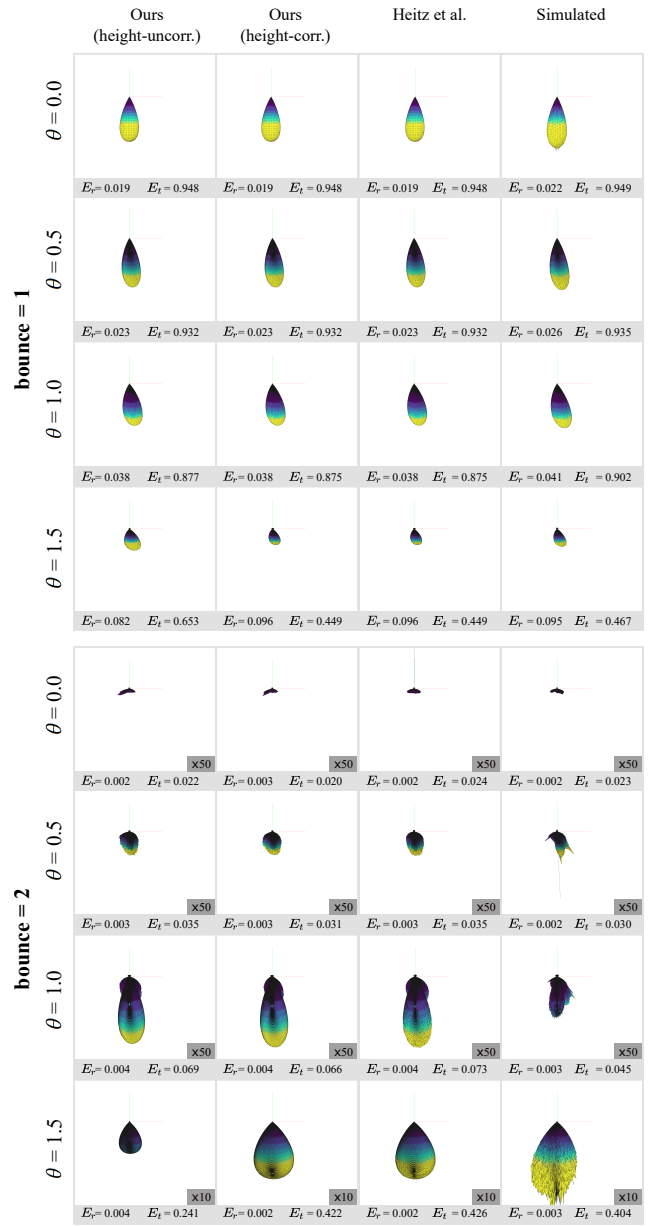


Fig. 15. Comparison between our multiple-bounce BxDF models (both height-uncorrelated and height-correlated), Heitz et al. [2016] model and simulated data, for rough dielectric material with roughness 1.0.  $\theta$  is the angle between the incident direction and the normal to the macrosurface.

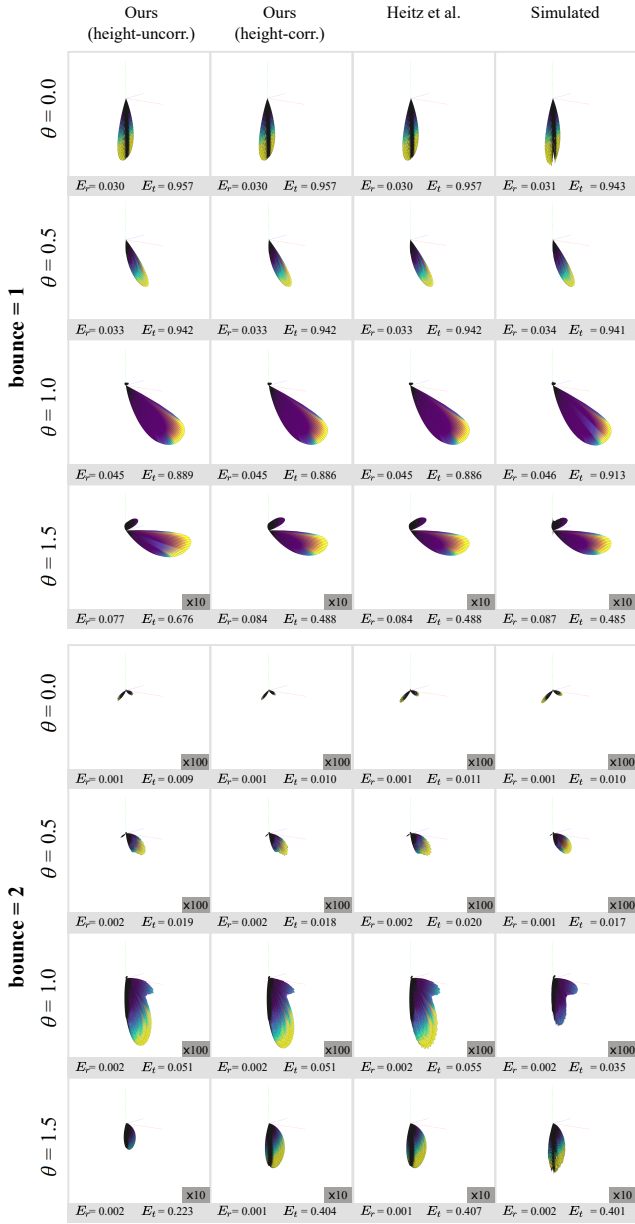


Fig. 16. Comparison between our multiple-bounce BSDF models (both height-uncorrelated and height-correlated), Heitz et al. [2016] model and simulated data, for anisotropic rough dielectric material with roughness 1.0 and 0.1.  $\theta$  is the angle between the incident direction and the normal to the macrosurface.

Thus, we have

$$s_i^{\text{forward}} = G_1^{\text{dist}}(-\mathbf{d}_i) = \frac{1}{1 + \Lambda(-\mathbf{d}_i)}. \quad (20)$$

Given a direction in the inverse path, as shown in Fig. 4 (right), its segment term is computed by:

$$s_i^{\text{inverse}} = e_i p_i, \quad (21)$$

$$\begin{aligned} e_i &= 1 - G_1(-\mathbf{d}_i, \frac{-\mathbf{d}_i + \mathbf{d}_{i+1}}{\|-\mathbf{d}_i + \mathbf{d}_{i+1}\|}) = 1 - G_1^{\text{dist}}(-\mathbf{d}_i) \\ &= 1 - \frac{1}{1 + \Lambda(-\mathbf{d}_i)} = \frac{\Lambda(-\mathbf{d}_i)}{1 + \Lambda(-\mathbf{d}_i)} \\ &= \frac{\Lambda(-\mathbf{d}_i)}{1 + \Lambda(-\mathbf{d}_i)}, \end{aligned} \quad (22)$$

$$\begin{aligned} p_i &= G_1(\mathbf{d}_i, \frac{-\mathbf{d}_{i-1} + \mathbf{d}_i}{\|-\mathbf{d}_{i-1} + \mathbf{d}_i\|}) \\ &= G_1^{\text{dist}}(\mathbf{d}_i) \\ &= \frac{-1}{1 + \Lambda(\mathbf{d}_i)} \\ &= \frac{1}{\Lambda(-\mathbf{d}_i)}. \end{aligned} \quad (23)$$

Thus, we have

$$\begin{aligned} s_i^{\text{inverse}} &= \frac{\Lambda(-\mathbf{d}_i)}{1 + \Lambda(-\mathbf{d}_i)} \frac{1}{\Lambda(-\mathbf{d}_i)} \\ &= \frac{1}{1 + \Lambda(-\mathbf{d}_i)} \\ &= s_i^{\text{forward}} \end{aligned} \quad (24)$$

Finally, we prove that the segment term has the reciprocity. Although the direction of  $\mathbf{d}_i$  is pointing downwards in our proof, the proof still holds, when it points upwards.

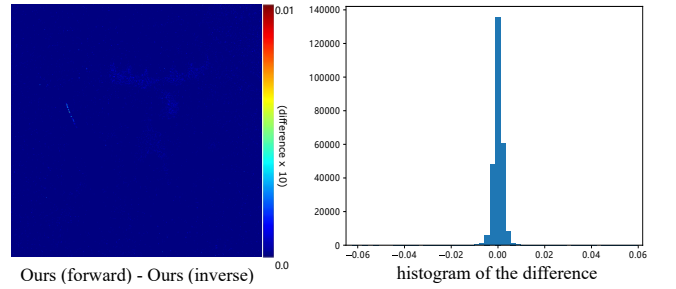


Fig. 17. The difference between renderings using  $\rho(\omega_i, \omega_o)$  and  $\rho(\omega_o, \omega_i)$ . The difference is because of the noise, rather than the model. We show the histogram of the difference. From its distribution, we can conclude that the expectation of the difference image is about zero.

## 2.2 Reciprocity of our height-correlated model

We use the same example as shown in Fig. 4, to demonstrate that our height-correlated model does not have reciprocity. Since the vertex terms are symmetric, the main reason for non-reciprocity is the segment term.

Given the forward path shown in Fig. 4 (left), the segment term is:

$$\begin{aligned} s_i^{\text{forward}} &= G_2^{(i < k)}(-\mathbf{d}_{i-1}, \mathbf{d}_i) G_2^{(i = k)}(-\mathbf{d}_i, \mathbf{d}_{i+1}) \\ &= G_1^{\text{dist}}(-\mathbf{d}_{i-1}) G_2^{\text{dist}}(-\mathbf{d}_i, \mathbf{d}_{i+1}) \\ &= \frac{1}{1 + \Lambda(-\mathbf{d}_{i-1})} \frac{1}{1 + \Lambda(-\mathbf{d}_i) + \Lambda(\mathbf{d}_{i+1})}. \end{aligned} \quad (25)$$

The segment term for the inverse path shown in Fig. 4 (right) is:

$$\begin{aligned} s_i^{\text{inverse}} &= G_2^{(i < k)}(-\mathbf{d}_i, \mathbf{d}_{i+1}) G_2^{(i = k)}(\mathbf{d}_i, -\mathbf{d}_{i-1}) \\ &= \left[ G_1^{\text{dist}}(\mathbf{d}_{i+1}) - G_2^{\text{dist}}(-\mathbf{d}_i, \mathbf{d}_{i+1}) \right] G_2^{\text{dist}}(\mathbf{d}_i, -\mathbf{d}_{i-1}) \\ &= \left[ \frac{1}{1 + \Lambda(\mathbf{d}_{i+1})} - \frac{1}{1 + \Lambda(\mathbf{d}_{i+1}) + \Lambda(-\mathbf{d}_i)} \right] \frac{1}{\Lambda(-\mathbf{d}_i) + \Lambda(-\mathbf{d}_{i-1})} \\ &= \frac{\Lambda(-\mathbf{d}_i)}{(1 + \Lambda(\mathbf{d}_{i+1}))(1 + \Lambda(\mathbf{d}_{i+1}) + \Lambda(-\mathbf{d}_i))} \frac{1}{\Lambda(-\mathbf{d}_i) + \Lambda(-\mathbf{d}_{i-1})}. \end{aligned} \quad (26)$$

Since  $s_i^{\text{forward}} \neq s_i^{\text{inverse}}$ , our height-correlated model does not have reciprocity.

### 3 LOBE VISUALIZATION

In Figs. 5 and the following eleven figures, we compare the visualized lobes for individual bounce between our methods (height-uncorrelated and height-correlated), Heitz et al. [2016] and simulated data which is obtained by ray tracing on a generated surface with Beckmann distribution [Heitz and Dupuy 2015]. We perform the comparison on rough diffuse (albedo set as 1), rough conductor (Fresnel set as 1) and rough dielectric BSDFs, considering both isotropic ( $\alpha = 0.25, 0.5, 1$ ) and anisotropic ( $\alpha = (1.0, 0.1)$ ) cases. We visualize the lobes with  $\omega_i$  elevation angles of 0.0, 0.5, 1.0 and 1.5 radians.  $E_r$  and  $E_t$  denote the total amount of reflected and transmitted energies, respectively.

For all the bounces with all the incident angles, our height-correlated model produces very similar results as Heitz et al. [2016], while our height-uncorrelated model has larger difference from Heitz et al. [2016] mostly at grazing angles.

### 4 CONVERGENCE VALIDATION

In Figure 18, we show the Mean Square Error (MSE) as a function of varying rendering time for our method (BDPT, height-correlated) and Heitz et al. [2016] in the Single Slab scene with varying roughness, considering directional lighting only. With only two samples per pixel, our method is able to produce very close result to the ground truth, while Heitz et al. [2016] produces result with a lot of noise. Increasing the number of samples (rendering time) improves the quality for both methods, but our method remains consistently better.

### REFERENCES

- Eric Heitz and Jonathan Dupuy. 2015. Implementing a Simple Anisotropic Rough Diffuse Material with Stochastic Evaluation. [https://drive.google.com/file/d/0BzvWIdpUpRx\\_M3ZmakxHYXZWaUk/view](https://drive.google.com/file/d/0BzvWIdpUpRx_M3ZmakxHYXZWaUk/view).
- Eric Heitz, Johannes Hanika, Eugene d'Eon, and Carsten Dachsbacher. 2016. Multiple-Scattering Microfacet BSDFs with the Smith Model. *ACM Trans. Graph.* 35, 4, Article 58 (July 2016), 14 pages.

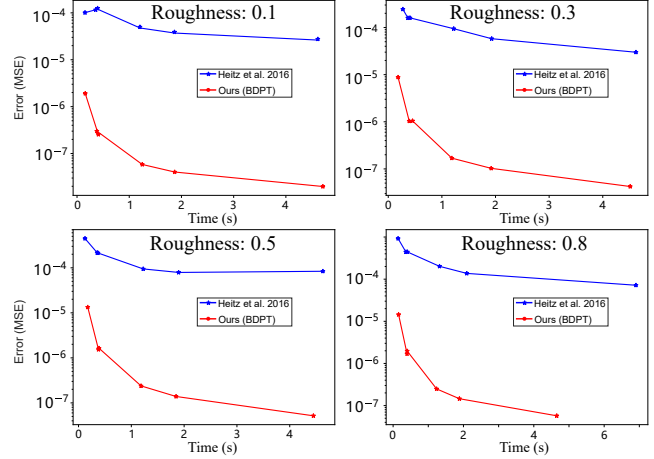


Fig. 18. The error (MSE) with logarithm scale of our method (height-correlated) and Heitz et al. [2016] over varying rendering time on the Single Slab scene with varying roughness.

- Vincent Ross, Denis Dion, and Guy Potvin. 2005. Detailed analytical approach to the Gaussian surface bidirectional reflectance distribution function specular component applied to the sea surface. *J. Opt. Soc. Am. A* 22, 11 (Nov. 2005), 2442–2453.
- B. Smith. 1967. Geometrical shadowing of a random rough surface. *IEEE Transactions on Antennas and Propagation* 15, 5 (1967), 668–671.